Has focused denudation sustained active thrusting at the Himalayan topographic front?

Cameron W. Wobus
Kip V. Hodges
Kelin X. Whipple
Department of Earth, Atmospheric and Planetary Sciences, Massachusetts Institute of Technology, Cambridge, Massachusetts 02139, USA

ABSTRACT

The geomorphic character of major river drainages in the Himalayan foothills of central Nepal suggests the existence of a discrete, west-northwest–trending break in rock uplift rates that does not correspond to previously mapped faults. The $^{40}Ar/^{39}Ar$ thermochronologic data from detrital muscovites with provenance from both sides of the discontinuity indicate that this geomorphic break also corresponds to a major discontinuity in cooling ages: samples to the south are Proterozoic to Paleozoic, whereas those to the north are Miocene and younger. Combined, these observations virtually require recent (Pliocene–Holocene) motion on a thrust-sense shear zone in the central Nepal Himalaya, ~20–30 km south of the Main Central thrust. Field observations are consistent with motion on a broad shear zone subparallel to the fabric of the Lesser Himalayan lithotectonic sequence. The results suggest that motion on thrusts in the toe of the Himalayan wedge may be synchronous with deeper exhumation on more hinterland structures in central Nepal. We speculate that this continued exhumation in the hinterland may be related to intense, sustained erosion driven by focused orographic precipitation at the foot of the High Himalaya.

Keywords: tectonics, Himalayas, Nepal, geomorphology, argon-argon, Main Central thrust.

INTRODUCTION

Recent geodynamic modeling of orogenic growth has led to the provocative hypothesis that erosion may exert first-order control on orogen-scale tectonics (e.g., Beaumont et al., 2001). However, direct field evidence of this feedback is not easily obtained. Here we present evidence for recent thrusting in the Himalayan hinterland at the position of the major topographic break between the physiographic lesser and higher Himalaya. Combined with evidence for Pliocene activity on the Main Central thrust (e.g., Harrison et al., 1997; Catlos et al., 2001; Robinson et al., 2003), our data imply sustained out-of-sequence thrusting that is suggestive of a direct link between tectonics and the monsoon-driven erosion of the High Himalaya.

We utilize the geomorphology of the Burhi Gandaki and Trisuli watersheds in central Nepal—derived from a 90 m digital elevation model (DEM) and observations on the ground—to identify breaks in hillslope, valley, and channel morphologies that may reflect unmapped, active structures in this area. All of the geomorphic observations suggest a narrowly distributed decrease in rock uplift rates from north to south, centered ~20–30 km south of the Main Central thrust zone. The $^{40}Ar/^{39}Ar$ thermochronologic data from detrital muscovites also indicate a major break in cooling ages at this location, implying a significant change in exhumation rates across a 10-km-wide zone. The simplest explanation for all of the data is a tectonic model including Pliocene–Holocene thrusting on a surface-breaking shear zone near the base of the High Himalaya in central Nepal.

GEOLOGIC SETTING

The Burhi Gandaki and Trisuli Rivers carve through the High Himalaya ~80 km northwest of Kathmandu, Nepal (Fig. 1). Their upper reaches traverse primarily Neoproterozoic rocks of the Tibetan Sedimentary Sequence, which are bounded at their base by predominantly normal-sense structures of the South Tibetan fault system. Downstream (south) of the South Tibetan fault system, and for most of their courses, the rivers carve steep-walled gorges through the high-grade metamorphic core of the range, represented by the Greater Himalayan Sequence. The Greater Himalayan Sequence is bounded at its base by the Main Central thrust zone, a crustal-scale feature that can be traced nearly the entire length of the Himalayan orogen (e.g., Hodges, 2000). In the footwall of the Main Central thrust zone, the rivers traverse the Lesser Himalayan Sequence, which is dominated in central Nepal by phyllites, quartzites, psammites, and metacarbonates of the Kuncha Formation (e.g., Stöcklin, 1980). Recent studies suggest that there may be significant repetition of the Kuncha section along foliation-parallel thrusts (e.g., DeCelles et al., 2001).

The steep-walled gorges typical of the Greater Himalayan Sequence persist within the Lesser Himalayan Sequence for ~20–30 km south of the Main Central thrust zone. Both rivers then cross a prominent physiographic transition, uncorrelated with any mapped structures or change in rock type, referred to as physiographic transition 2 (PT_2) by Hodges et al. (2001). PT_2 is characterized by a number of changes in landscape morphology, including (1) a change from narrow, steep-walled gorges in the north to wide, alluviated valleys in the south; (2) an abrupt decrease in hillslope gradient from north to south (Fig. 1); (3) an abrupt transition from fresh, landslide-covered hillslopes in the north to deeply weathered, red soils on hillslopes and channel banks; (4) an abrupt appearance from north to south of thick (to 200 m) fluvial fill terraces in both drainages; and (5) an abrupt decrease in channel gradient from north to south, discussed in more detail herein. All of these observations suggest a profound and narrowly distributed decrease in the rates of denudation from north to south.

Noting the existence and position of this physiographic transition throughout the Him-

© 2003 Geological Society of America. For permission to copy, contact Copyright Permissions, GSA, or editing@geosociety.org.

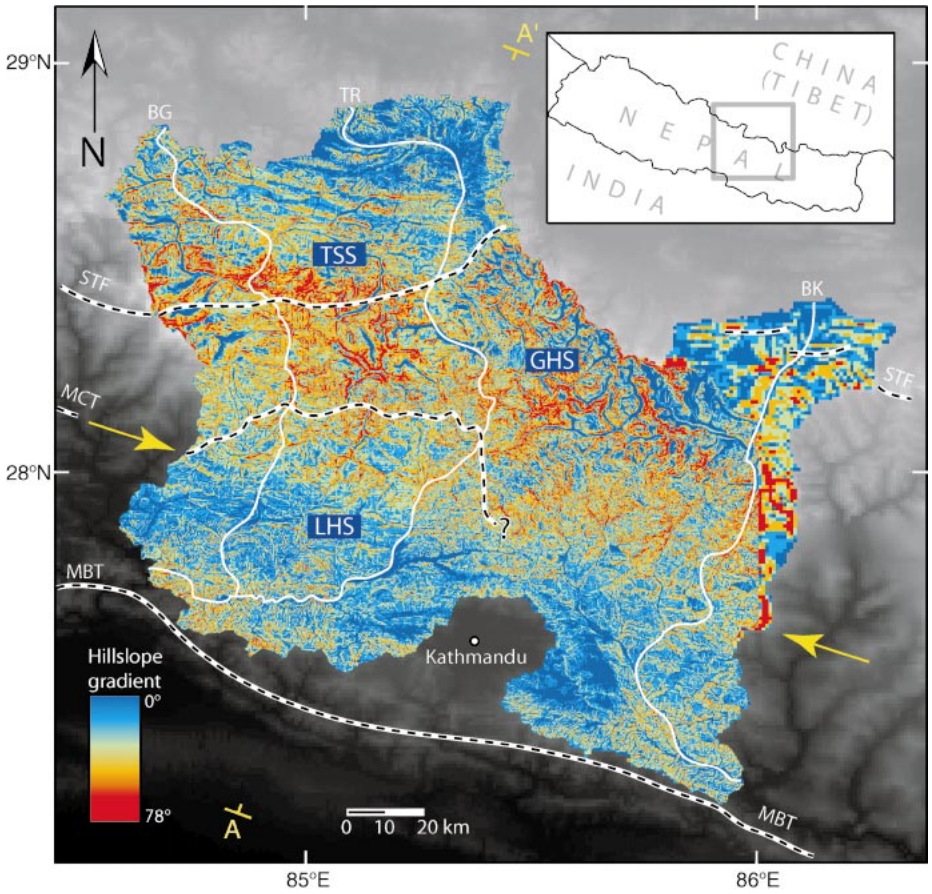

Figure 1. Site location map (inset) and slope map for study area. Physiographic transition, PT_2, is prominent break in hillslope gradient between yellow arrows. Structural and lithotectonic units: TSS—Tibetan Sedimentary Sequence; GHS—Greater Himalayan Sequence; LHS—Lesser Himalayan Sequence;. Rivers: BG—Burhi Gandaki; TR—Trisuli; BK—Bhote Kosi. Section A–A′ is shown in Figure 2. Fault locations are approximated from Colchen et al. (1986), Searle et al. (1997), Macfarlane et al. (1992), and Hodges (2000).

alaya, Seeber and Gornitz (1983) suggested that it may be indicative of recent movement on the Main Central thrust system. However, this interpretation runs counter to the generally agreed upon developmental sequence for major thrust fault systems in the Himalaya. For example, the Main Central thrust system is thought to have been active ca. 30–23 Ma, with shortening progressing southward to the Main Boundary thrust system in late Miocene–Pliocene time and to the Main Frontal thrust system in Pliocene–Holocene time (e.g., Hodges, 2000). Implicit in this model is the assumption that the Main Central thrust became inactive as deformation stepped southward.

With this assumption, tectonic models of the Nepal Himalaya typically invoke a ramp-flat geometry on the basal décollement, or Himalayan sole thrust, to explain the prominent physiographic transition (e.g., Cattin and Avouac, 2000) (Fig. 2A). Alternatively, PT_2 may be an expression of recent motion on the Main Central thrust through much of Nepal (e.g., Seeber and Gornitz, 1983), or on unmapped structures farther to the south in the Burhi Gandaki and Trisuli watersheds (Fig. 2B). Such out-of-sequence thrusting is relatively common in fold-and-thrust belts, and is predicted by many kinematic models as a way of preserving the critical taper of accretionary wedges with strong erosion gradients between the foreland and the hinterland (e.g., Dahlen and Suppe, 1988). Data from microseismicity and geodetics have been invoked as evidence for the ramp-flat model (e.g., Pandey et al., 1999; Bilham et al., 1997); however, these data are equally consistent with surface-breaking structures at PT_2. Thermochronologic and thermobarometric data suggest varied types of activity on the Main Central thrust as recently as the early Pliocene, lending additional support to the hypothesis of reactivated hinterland structures (e.g., Macfarlane et al., 1992; Harrison et al., 1997; Catlos et al., 2001).

If PT_2 marks the locus of out-of-sequence thrusting rather than the position of a buried ramp in the Himalayan sole thrust, PT_2 would be expected to correspond with an abrupt change in rock uplift rates. In the following, a combination of stream-profile analysis and $^{40}Ar/^{39}Ar$ thermochronology is used to test this prediction.

METHODS AND RESULTS

Stream Profiles

In a variety of natural settings, empirical data from river channels exhibit a scaling in which local channel slope can be expressed as a power-law function of contributing drainage

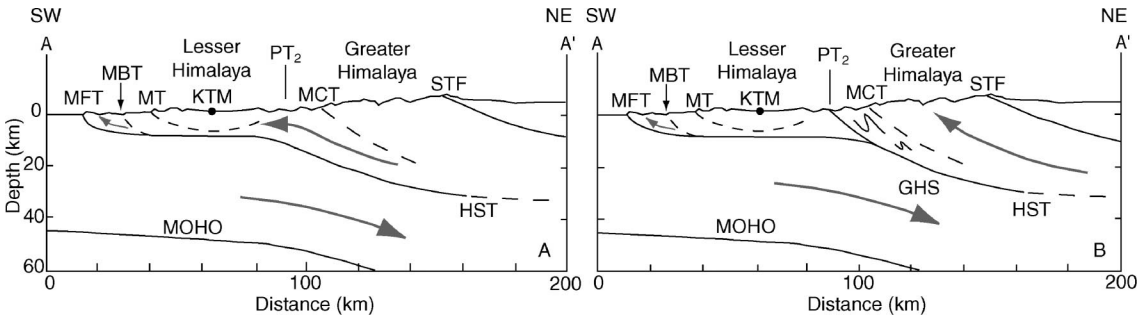

Figure 2. Two interpretations of Holocene tectonics of central Nepal. MFT—Main Frontal thrust; HST—Himalayan sole thrust; MT—Mahabarat thrust; KTM—Kathmandu; MBT—Main Boundary thrust; MCT—Main Central thrust; STF—South Tibetan fault system; GHS—Greater Himalayan Sequence; PT_2—physiographic transition 2. A: Passive transport over ramp in Himalayan sole thrust explains uplift gradients beneath PT_2; modern shortening is accommodated at toe of range (southwest end of cross section). B: Thrusting at Main Central thrust continues today, stepping forward to PT_2 in study area. Deep exhumation is confined to zone between South Tibetan fault system and PT_2, and décollement beneath Kathmandu is entirely thin skinned.

area (e.g., Howard and Kerby, 1983). Previous work suggests that the pre-exponential factor in this function—referred to as the steepness coefficient (k_s)—is positively correlated with the rock uplift rate U (e.g., Snyder et al., 2000). The exponent on drainage area—referred to as the concavity index (θ)—typically falls in a narrow range between 0.3 and 0.6, but may approach much higher values in zones of distributed uplift (e.g., Snyder et al., 2000; Kirby and Whipple, 2001). We stress that our quantitative understanding of feedbacks related to changes in channel width, hydraulic roughness, the quantity and caliber of abrasive tools, and the relative importance of various erosive processes remains limited (e.g., Lavé and Avouac, 2001; Sklar and Dietrich, 1998; Whipple et al., 2000). Moreover, we note that k_s also depends on many factors, including rock strength and climate, limiting our ability to derive quantitative estimates of uplift rates from slope versus area data. However, where rock erodibility is nearly invariant and climatic variability is smooth, abrupt changes in k_s may be confidently interpreted as reflecting a change in rock uplift rate.

Channel slope and drainage area data were extracted for 56 tributaries in the study area from a 90 m DEM of central Nepal. Using a reference concavity of 0.45 (e.g., Snyder et al., 2000), steepness coefficients derived from logarithmic plots of slope versus area range from 84 to 560 $m^{0.9}$. Channels having a source below PT_2 typically have uniformly low steepness values. Channels crossing PT_2 typically have low steepness values in the lowest reaches and approach the upper envelope of k_s values above PT_2. The trans-Himalayan trunk streams, including the Burhi Gandaki and Trisuli main stems, have high steepness values in their middle reaches, bounded above and below by sections having lower steepness (see Fig. DR-1[1]). In plan view, the boundary between high and low k_s values is nearly coincident with the break in hillslope gradients illustrated in Figure 1, suggesting that hillslopes and river channels may each be responding to a decrease in rock uplift rates from north to south (Fig. 3A). Although the Lesser Himalayan Sequence in the field area varies locally among phyllites, psammites, and metacarbonates, no systematic changes in rock character were observed at PT_2 in any of the drainages, suggesting that the transition from high to low steepness values is not a result of a change in rock erodibility (e.g., Snyder et al., 2000).

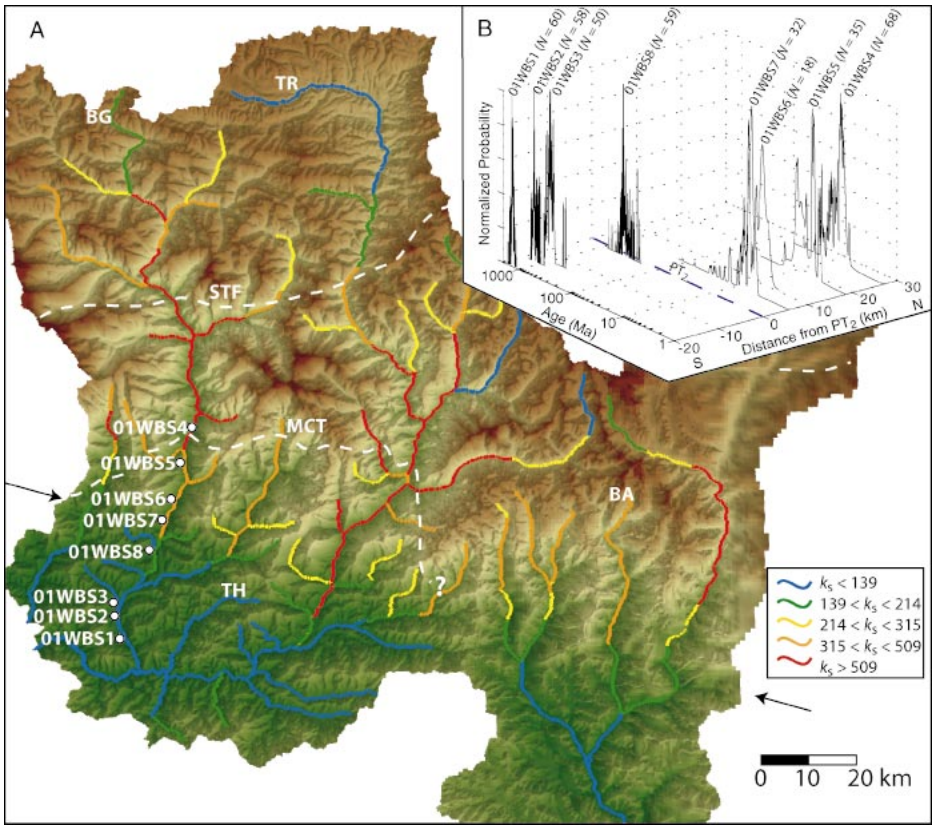

Figure 3. A: Distribution of k_s values for channel segments in study area (see text). Black arrows show position of physiographic transition PT_2, as in Figure 1. Rivers: BG—Burhi Gandaki; TR—Trisuli; TH—Thopal Khola; BA—Balephi Khola. Long profiles are available (see footnote 1 in text). White dots along Burhi Gandaki trunk stream show sediment sampling locations. B: Distribution of muscovite $^{40}Ar/^{39}Ar$ cooling ages for sediment samples. Apparent ages (*y* axis) are plotted on log scale for ease of presentation; peak of distribution for sample 01WBS7 is ~400 m.y. younger than peak for 01WBS8. Note tail on 01WBS7 distribution, indicating input of older material and possibly presence of both hanging-wall and footwall rocks from surface-breaking thrust within this catchment. Normalized probabilities (*z* axis) illustrate relative abundances of ages from each sample.

$^{40}Ar/^{39}Ar$ Thermochronology

Eight detrital samples were collected from small tributaries to the Burhi Gandaki for muscovite $^{40}Ar/^{39}Ar$ thermochronology (Fig. 3A). Selected tributary basins were oriented subparallel to PT_2 and the overall structural grain, ensuring that the sediment from each sample was derived from a similar tectonostratigraphic position. Basins were typically 20–25 km^2, with maximum across-strike basin widths ranging from 2 to 5 km. The northernmost sample was collected from the Burhi Gandaki trunk stream, to provide a view of cooling histories upstream of the Main Central thrust. Sampling locations span a distance of 47 km, as projected onto a line oriented at 19° east of north (approximately parallel to section A–A′ in Fig. 1).

Muscovites were separated by standard mineral-separation techniques prior to irradiation at the McMaster University nuclear reactor in Ontario, Canada. For each sample, 20–80 aliquots of muscovite were analyzed by laser microprobe, each consisting of between 1 and 20 grains. Many of the smaller aliquots had low radiogenic yields and therefore high uncertainties. Analyses reported here are limited to those with >50% radiogenic yield, reducing the total number of reported analyses to between 18 and 68. Complete data are available in the Data Repository (see footnote 1).

Figure 3B shows the normalized probability-density functions of sample ages plotted against distance from PT_2. South of PT_2, dates range from Mesoproterozoic to Paleozoic, with an apparent trend toward older ages from north to south. This trend may reflect partial loss of radiogenic ^{40}Ar from samples near PT_2 due to footwall heating beneath a thin thrust sheet in the early stages of Main Central thrust development (e.g., Arita et al., 1997). Argon release spectra from bedrock samples south of PT_2 and in the Kathmandu nappe are consistent with this hypothesis (e.g., Copeland et al., 1991, personal commun.). North of PT_2, nearly all dates are Miocene or younger. The ~400 m.y. break in cooling ages at PT_2 suggests a major discontinuity in rock uplift rates across the physiographic transition. Furthermore, the

[1]GSA Data Repository item 2003131, stream profiles and thermochronologic data, is available online at www.geosociety.org/pubs/ft2003.htm, or on request from editing@geosociety.org or Documents Secretary, GSA, P.O. Box 9140, Boulder, CO 80301-9140, USA.

age distributions south of PT_2 require that none of the samples below PT_2 have undergone prolonged heating above ~350 °C during Himalayan orogenesis. This result seems inconsistent with tectonic models that require prolonged transport of the Main Central thrust hanging wall over a ramp on the Himalayan sole thrust, with a geometry as envisioned by Pandey et al. (1999) or Cattin and Avouac (2000).

Field Observations

Limited outcrop in the field area and a lack of marker beds in the Kuncha Formation phyllites limit our ability to constrain unequivocally the position of a thrust at PT_2. Any new thrusts in this setting are also likely to be parallel to—and thus difficult to deconvolve from—the more pervasive Himalayan fabric (nominally west-northwest trending and dipping north at 30°–50°). Despite these limitations, however, a number of structural observations are consistent with the presence of a surface-breaking thrust at PT_2, including (1) numerous small-scale shear zones subparallel to and crosscutting the structural grain within the Kuncha Formation phyllites, (2) hydrothermal activity in tributary valleys along PT_2, and (3) large-scale changes in bedrock attitudes in outcrop at the scale of tens to hundreds of meters.

DISCUSSION AND CONCLUSIONS

All of the data indicate a major change in rock uplift rates and thermal history in central Nepal, centered ~20–30 km south of the Main Central thrust. The tectonic picture that emerges for central Nepal is therefore one in which activity at the frontal thrusts today (e.g., Main Boundary thrust and Main Frontal thrust) may be synchronous with motion on structures farther hinterland (e.g., Main Central thrust and at PT_2). Previous work has suggested that modern activity on or near the Main Central thrust may be favored by extreme topographic gradients between the Tibetan Plateau and the Indian foreland (e.g., Hodges et al., 2001; Grujic et al., 2002). In central Nepal, the Main Central thrust forms a major reentrant to the north, in contrast to its more linear trend farther to the west (see Fig. 1). This geometric relationship may have favored the initiation of a new shear zone at PT_2, parallel to the regional trend of the Main Central thrust and the pervasive structural grain.

Intense precipitation at the southern front of the High Himalaya is also likely to play a role in the kinematics of the Himalayan fold-and-thrust belt, and may have been important in maintaining a locus of active thrusting at PT_2 (e.g., Dahlen and Suppe, 1988). As the summer monsoons approach the Tibetan Plateau, orographic focusing of precipitation results in strong north-south gradients in rainfall, which increases surface denudation rates on the windward side of the range. Coupled with extreme topographic gradients and continued convergence between India and Eurasia, this strong precipitation may have resulted in sustained focusing of exhumation along the metamorphic core of the Himalaya (e.g., Beaumont et al., 2001), rather than a complete transfer of shortening to the Main Boundary thrust and Main Frontal thrust. The combined geomorphic, thermochronologic, and field evidence for an active shear zone at the foot of the Himalaya may therefore provide evidence for erosionally driven rock uplift at the orogen scale.

ACKNOWLEDGMENTS

We thank F. Pazzaglia and P. DeCelles for constructive reviews of the original manuscript, and B. Crosby, K. Ruhl, T. Schildgen, and N. Wobus for assistance in the field. Logistical support was provided by Himalayan Experience. Work was supported by National Science Foundation grant EAR-008758.

REFERENCES CITED

Arita, K., Dallmeyer, R.D., and Takasu, A., 1997, Tectonothermal evolution of the Lesser Himalaya, Nepal: Constraints from $^{40}Ar/^{39}Ar$ ages from the Kathmandu Klippe: The Island Arc, v. 6, p. 372–384.

Beaumont, C., Jamieson, R.A., Nguyen, M.H., and Lee, B., 2001, Himalayan tectonics explained by extrusion of a low-viscosity crustal channel coupled to focused surface denudation: Nature, v. 414, p. 738–742.

Bilham, R., Larson, K., Freymuller, J., and Members, P.I., 1997, GPS measurements of present-day convergence across the Nepal Himalaya: Nature, v. 386, p. 61–64.

Catlos, E.J., Harrison, T.M., Kohn, M.J., Grove, M., Ryerson, F.J., Manning, C.E., and Upreti, B.N., 2001, Geochronologic and thermobarometric constraints on the evolution of the Main Central thrust, central Nepal Himalaya: Journal of Geophysical Research, v. 106, no. B8, p. 16,177–16,204.

Cattin, R., and Avouac, J.P., 2000, Modeling mountain building and the seismic cycle in the Himalaya of Nepal: Journal of Geophysical Research, v. 105, p. 13,389–13,407.

Colchen, M., Le Fort, P., and Pêcher, A., 1986, Recherches géologiques dans l'Himalaya du Népal, Annapurna–Manaslu–Ganesh Himal: Paris, Centre National de la Recherche Scientifique, 136 p.

Copeland, P., Harrison, T.M., Hodges, K.V., Maruejol, P., Le Fort, P., and Pecher, A., 1991, An early Pliocene thermal disturbance of the Main Central thrust, central Nepal: Implications for Himalayan tectonics: Journal of Geophysical Research, v. 96, p. 8475–8500.

Dahlen, F.A., and Suppe, J., 1988, Mechanics, growth, and erosion of mountain belts, *in* Clark, S.P.J., et al., eds., Processes in continental lithospheric deformation: Geological Society of America Special Paper 218, p. 161–178.

DeCelles, P.G., Robinson, D.M., Quade, J., Ojha, T.P., Garzione, C.N., Copeland, P., and Upreti, B.N., 2001, Stratigraphy, structure, and tectonic evolution of the Himalayan fold-thrust belt in western Nepal: Tectonics, v. 20, p. 487–509.

Grujic, D., Hollister, L.S., and Parrish, R.R., 2002, Himalayan metamorphic sequence as an orogenic channel: Insight from Bhutan: Earth and Planetary Science Letters, v. 198, p. 177–191.

Harrison, T.M., Ryerson, F.J., Le Fort, P., Yin, A., Lovera, O., and Catlos, E.J., 1997, A late Miocene–Pliocene origin for the central Himalayan inverted metamorphism: Earth and Planetary Science Letters, v. 146, p. E1–E7.

Hodges, K.V., 2000, Tectonics of the Himalaya and southern Tibet from two perspectives: Geological Society of America Bulletin, v. 112, p. 324–350.

Hodges, K.V., Hurtado, J.M., and Whipple, K.X., 2001, Southward extrusion of Tibetan crust and its effect on Himalayan tectonics: Tectonics, v. 20, p. 799–809.

Howard, A.D., and Kerby, G., 1983, Channel changes in badlands: Geological Society of America Bulletin, v. 94, p. 739–752.

Kirby, E., and Whipple, K.X., 2001, Quantifying differential rock-uplift rates via stream profile analysis: Geology, v. 29, p. 415–418.

Lavé, J., and Avouac, J.P., 2001, Fluvial incision and tectonic uplift across the Himalayas of central Nepal: Journal of Geophysical Research, v. 106, p. 26,561–26,591.

Macfarlane, A., Hodges, K.V., and Lux, D., 1992, A structural analysis of the Main Central thrust zone, Langtang National Park, central Nepal Himalaya: Geological Society of America Bulletin, v. 104, p. 1389–1402.

Pandey, M.R., Tandukar, R.P., Avouac, J.P., Vergne, J., Heritier, T., Le Fort, P., and Upreti, B.N., 1999, Seismotectonics of the Nepal Himalaya from a local seismic network: Journal of Asian Earth Sciences, v. 17, p. 703–712.

Robinson, D.M., DeCelles, P.G., Garzione, C.N., Pearson, O.N., Harrison, T.M., and Catlos, E.J., 2003, Kinematic model for the Main Central thrust in Nepal: Geology, v. 31, p. 359–362.

Searle, M.P., Parrish, R.R., Hodges, K.V., Hurford, A., Ayres, M.W., and Whitehouse, M.J., 1997, Shisha Pangma leucogranite, South Tibetan Himalaya: Field relations, geochemistry, age, origin, and emplacement: Journal of Geology, v. 105, p. 295–317.

Seeber, L., and Gornitz, V., 1983, River profiles along the Himalayan arc as indicators of active tectonics: Tectonophysics, v. 92, p. 335–367.

Sklar, L., and Dietrich, W.E., 1998, River longitudinal profiles and bedrock incision models: Stream power and the influence of sediment supply, *in* Tinkler, K.J., and Wohl, E.E., eds., Rivers over rock: Fluvial processes in bedrock channels: American Geophysical Union Geophysical Monograph 107, p. 237–260.

Snyder, N., Whipple, K., Tucker, G., and Merritts, D., 2000, Landscape response to tectonic forcing: DEM analysis of stream profiles in the Mendocino triple junction region, northern California: Geological Society of America Bulletin, v. 112, p. 1250–1263.

Stöcklin, J., 1980, Geology of Nepal and its regional frame: Geological Society [London] Journal, v. 137, p. 1–34.

Whipple, K.X., Hancock, G.S., and Anderson, R.S., 2000, River incision into bedrock: Mechanics and relative efficacy of plucking, abrasion, and cavitation: Geological Society of America Bulletin, v. 112, p. 490–503.

Manuscript received 15 April 2003
Revised manuscript received 5 June 2003
Manuscript accepted 6 June 2003

Printed in USA

Table DR-1
40Ar/39Ar Data for Detrital Muscovites
Burhi Gandaki River - Sample 01WBS1

Analysis Number	$^{36}Ar/^{40}Ar$ $(x10^{-5})^{++}$	$^{39}Ar/^{40}Ar$ $(x10^{-3})^{++}$	$^{39}Ar_K$ $(x10^{-16}$ mol$)^{**}$	$^{40}Ar^{*}$ $(\%)^{\#}$	Age (Ma)$^{\$}$
1	2.53 (1.41)	1.45 (0.008)	5.065	99.3	1456.17 ± 8.88 (5.31)
2	0.02 (2.47)	1.43 (0.001)	3.643	100.0	1478.16 ± 7.21 (0.61)
3	0.55 (1.91)	1.39 (0.002)	4.820	99.8	1509.76 ± 7.51 (1.82)
4	13.81 (2.11)	1.48 (0.000)	5.999	95.9	1403.26 ± 6.95 (0.14)
5	22.16 (3.20)	1.58 (0.005)	3.988	93.5	1316.55 ± 7.49 (3.44)
6	12.33 (3.08)	1.61 (0.009)	7.292	96.4	1328.79 ± 8.49 (5.22)
7	15.79 (2.99)	1.72 (0.006)	6.092	95.3	1258.47 ± 7.31 (3.44)
8	18.47 (1.60)	1.56 (0.010)	4.741	94.5	1338.43 ± 9.10 (6.12)
9	26.70 (5.23)	1.73 (0.015)	3.620	92.1	1221.21 ± 10.58 (8.48)
10	19.73 (1.74)	1.36 (0.004)	3.853	94.2	1468.69 ± 7.68 (2.79)
11	2.94 (5.43)	1.34 (0.004)	3.810	99.1	1537.21 ± 8.07 (3.29)
12	1.94 (2.62)	1.59 (0.009)	4.964	99.4	1368.79 ± 8.59 (5.20)
13	2.41 (1.32)	1.64 (0.007)	5.727	99.3	1335.67 ± 7.83 (4.02)
14	3.64 (3.04)	1.29 (0.009)	3.545	98.9	1571.75 ± 10.72 (7.68)
15	4.34 (4.12)	1.25 (0.007)	3.679	98.7	1604.37 ± 9.43 (5.62)
16	3.70 (2.13)	1.24 (0.010)	2.392	98.9	1616.35 ± 11.49 (8.62)
17	4.64 (3.31)	1.30 (0.006)	4.029	98.6	1565.26 ± 8.97 (4.98)
18	5.95 (5.40)	1.40 (0.005)	2.850	98.2	1483.80 ± 8.25 (4.03)
19	3.24 (3.00)	1.48 (0.005)	4.068	99.0	1433.53 ± 7.91 (3.59)
20	4.39 (3.47)	1.56 (0.013)	4.726	98.7	1377.53 ± 10.40 (7.82)
21	5.69 (2.04)	1.46 (0.023)	7.312	98.3	1439.18 ± 17.31 (15.80)
22	0.04 (2.16)	1.46 (0.004)	7.159	100.0	1455.94 ± 7.65 (2.80)
23	0.37 (0.91)	1.57 (0.016)	6.656	99.9	1384.63 ± 12.09 (9.93)
24	0.22 (1.29)	1.59 (0.033)	5.816	99.9	1371.95 ± 20.84 (19.68)
25	0.34 (3.00)	1.55 (0.016)	5.999	99.9	1400.33 ± 12.24 (10.08)
26	7.20 (1.78)	1.52 (0.024)	5.906	97.9	1398.05 ± 16.89 (15.40)
27	0.18 (2.25)	1.56 (0.021)	6.291	99.9	1395.05 ± 14.96 (13.26)
28	6.81 (2.74)	1.68 (0.039)	6.962	98.0	1305.65 ± 22.83 (21.84)
29	0.26 (2.06)	1.47 (0.018)	5.648	100.0	1451.87 ± 14.33 (12.44)
30	1.87 (2.71)	1.62 (0.040)	4.982	99.4	1351.03 ± 24.36 (23.40)
31	2.32 (1.60)	1.44 (0.021)	4.853	99.3	1464.00 ± 16.38 (14.74)
32	3.25 (2.67)	1.54 (0.047)	4.026	99.0	1393.27 ± 30.72 (29.93)
33	1.75 (1.83)	1.44 (0.025)	4.719	99.5	1463.49 ± 18.59 (17.17)
34	4.66 (0.76)	1.41 (0.005)	3.753	98.6	1479.65 ± 8.22 (3.99)
35	2.63 (3.53)	1.49 (0.026)	5.754	99.2	1429.37 ± 18.58 (17.20)
36	4.74 (0.68)	1.53 (0.018)	5.743	98.6	1401.00 ± 13.51 (11.59)
37	1.85 (3.04)	1.40 (0.017)	6.676	99.5	1491.90 ± 14.51 (12.58)
38	2.15 (3.24)	1.49 (0.029)	3.830	99.4	1433.82 ± 20.47 (19.21)
39	3.03 (3.26)	1.42 (0.014)	4.877	99.1	1477.40 ± 12.29 (9.97)
40	3.02 (5.15)	1.35 (0.002)	3.019	99.1	1529.79 ± 7.60 (1.95)
41	13.14 (2.77)	1.46 (0.018)	4.437	96.1	1418.76 ± 14.56 (12.76)
42	13.44 (2.90)	1.44 (0.028)	4.296	96.0	1431.52 ± 21.13 (19.92)
43	15.65 (5.42)	1.39 (0.021)	3.558	95.4	1459.53 ± 17.39 (15.86)
44	10.18 (1.92)	1.40 (0.016)	5.543	97.0	1472.71 ± 13.89 (11.90)
45	15.07 (1.80)	1.35 (0.008)	3.587	95.5	1494.86 ± 9.54 (6.22)
46	9.02 (1.34)	1.35 (0.003)	6.032	97.3	1513.85 ± 7.60 (2.13)
47	15.63 (4.58)	1.43 (0.017)	3.639	95.4	1431.53 ± 14.16 (12.29)
48	19.30 (3.12)	1.58 (0.004)	3.238	94.3	1326.00 ± 7.33 (2.99)
49	11.32 (2.51)	1.46 (0.011)	5.126	96.7	1427.07 ± 10.45 (7.73)
50	16.05 (2.49)	1.48 (0.009)	3.683	95.3	1393.63 ± 9.09 (5.90)
51	12.56 (4.55)	1.48 (0.013)	4.613	96.3	1405.88 ± 11.46 (9.11)
52	15.76 (5.14)	1.49 (0.002)	3.690	95.3	1389.99 ± 7.10 (1.64)
53	18.40 (3.84)	1.23 (0.002)	2.642	94.6	1574.48 ± 7.80 (2.21)
54	0.20 (2.88)	1.26 (0.007)	4.680	100.0	1614.93 ± 9.64 (5.93)
55	11.65 (4.01)	1.54 (0.011)	5.248	96.6	1371.17 ± 9.72 (6.91)
56	15.08 (3.16)	1.38 (0.012)	3.585	95.5	1465.76 ± 11.86 (9.46)
57	13.05 (2.93)	1.46 (0.014)	4.361	96.1	1422.05 ± 12.38 (10.20)
58	10.51 (1.10)	1.41 (0.006)	5.235	96.9	1458.26 ± 8.56 (4.75)
59	18.62 (4.00)	1.06 (0.010)	2.231	94.5	1736.08 ± 13.45 (10.85)
60	16.25 (5.33)	1.15 (0.006)	2.776	95.2	1652.34 ± 9.48 (5.52)

Table DR-1
40Ar/39Ar Data for Detrital Muscovites
Burhi Gandaki River - Sample 01WBS2

Analysis Number	$^{36}Ar/^{40}Ar$ $(x10^{-5})^{++}$	$^{39}Ar/^{40}Ar$ $(x10^{-3})^{++}$	$^{39}Ar_K$ $(x10^{-16}$ mol$)^{**}$	$^{40}Ar^*$ $(\%)^{\#}$	Age (Ma)$^{\$}$
1	3.86 (3.44)	1.71 (0.011)	4.924	98.9	1292.90 ± 8.78 (5.81)
2	23.60 (12.85)	2.82 (0.022)	1.714	93.0	845.87 ± 7.47 (5.72)
3	3.06 (2.51)	1.70 (0.008)	5.175	99.1	1300.42 ± 7.89 (4.33)
4	2.65 (1.84)	1.47 (0.006)	6.288	99.2	1440.70 ± 8.16 (4.07)
5	2.55 (1.19)	1.78 (0.008)	7.802	99.2	1260.67 ± 7.65 (4.09)
6	2.65 (3.13)	2.33 (0.018)	9.452	99.2	1034.70 ± 8.39 (6.23)
7	3.04 (2.71)	1.71 (0.014)	5.312	99.1	1297.72 ± 10.08 (7.63)
8	4.24 (1.81)	2.02 (0.007)	7.681	98.7	1147.66 ± 6.80 (3.10)
9	2.85 (3.87)	1.63 (0.005)	8.386	99.2	1341.57 ± 7.44 (3.14)
10	3.20 (0.77)	2.43 (0.007)	12.496	99.1	999.17 ± 5.85 (2.08)
11	20.82 (3.45)	1.96 (0.007)	5.194	93.8	1128.85 ± 6.86 (3.37)
12	14.72 (2.57)	1.87 (0.008)	6.994	95.6	1185.31 ± 7.30 (3.86)
13	1.42 (1.36)	1.97 (0.015)	7.540	99.6	1174.83 ± 9.16 (6.79)
14	2.34 (2.30)	1.98 (0.013)	6.065	99.3	1167.95 ± 8.47 (5.85)
15	16.30 (2.53)	1.87 (0.024)	6.344	95.2	1180.95 ± 13.40 (11.89)
16	11.11 (2.51)	2.11 (0.007)	10.500	96.7	1092.59 ± 6.41 (2.64)
17	0.63 (0.93)	2.16 (0.014)	6.961	99.8	1099.60 ± 7.83 (5.19)
18	16.07 (2.55)	2.36 (0.020)	8.105	95.3	991.51 ± 8.77 (6.88)
19	19.15 (2.48)	2.12 (0.010)	6.127	94.3	1067.92 ± 6.95 (3.92)
20	14.67 (4.81)	2.25 (0.017)	8.483	95.7	1031.69 ± 8.46 (6.34)
21	6.83 (1.01)	1.85 (0.000)	9.548	98.0	1215.25 ± 6.30 (0.10)
22	9.31 (3.66)	1.66 (0.026)	6.238	97.2	1307.07 ± 16.59 (15.21)
23	8.47 (1.93)	1.99 (0.030)	8.311	97.5	1148.33 ± 14.29 (12.95)
24	6.84 (1.33)	1.89 (0.000)	9.764	98.0	1195.52 ± 6.23 (0.14)
25	8.82 (2.08)	1.79 (0.018)	7.156	97.4	1239.23 ± 11.24 (9.26)
26	0.37 (0.90)	1.52 (0.039)	7.772	99.9	1418.96 ± 26.17 (25.22)
27	10.83 (3.76)	1.71 (0.014)	5.555	96.8	1277.78 ± 10.31 (7.98)
28	0.06 (1.57)	1.57 (0.010)	6.596	100.0	1388.64 ± 9.32 (6.26)
29	10.00 (2.53)	1.54 (0.016)	5.388	97.0	1376.81 ± 12.40 (10.33)
30	9.94 (2.07)	1.63 (0.035)	5.730	97.1	1323.07 ± 21.76 (20.71)
31	13.43 (4.24)	1.36 (0.008)	3.162	96.0	1489.57 ± 9.47 (6.13)
32	6.02 (1.48)	1.83 (0.000)	9.422	98.2	1228.89 ± 6.35 (0.13)
33	0.77 (0.59)	1.68 (0.000)	8.636	99.8	1322.94 ± 6.68 (0.17)
34	8.95 (1.49)	1.62 (0.012)	5.567	97.4	1330.35 ± 9.69 (7.00)
35	10.44 (1.61)	1.68 (0.033)	4.963	96.9	1291.05 ± 19.78 (18.66)
36	9.62 (2.23)	1.59 (0.010)	5.087	97.2	1348.23 ± 8.98 (5.90)
37	10.82 (3.30)	1.58 (0.061)	4.516	96.8	1350.35 ± 38.44 (37.84)
38	7.34 (3.01)	1.65 (0.015)	6.921	97.8	1320.82 ± 10.79 (8.48)
39	7.72 (0.81)	1.50 (0.015)	5.989	97.7	1405.88 ± 11.90 (9.66)
40	9.39 (2.03)	1.71 (0.016)	7.412	97.2	1279.01 ± 10.76 (8.55)
41	17.19 (1.78)	1.43 (0.006)	3.373	94.9	1424.44 ± 8.13 (4.10)
42	11.33 (3.91)	1.67 (0.027)	5.996	96.7	1294.86 ± 16.70 (15.35)
43	10.29 (1.36)	1.68 (0.031)	6.633	97.0	1292.35 ± 18.52 (17.31)
44	12.69 (2.05)	1.36 (0.017)	4.330	96.2	1491.37 ± 14.71 (12.81)
45	8.52 (1.46)	1.75 (0.019)	8.321	97.5	1261.59 ± 11.88 (9.97)
46	9.00 (1.59)	1.75 (0.014)	7.900	97.3	1257.36 ± 10.00 (7.64)
47	9.24 (2.76)	1.63 (0.003)	7.145	97.3	1322.57 ± 6.98 (2.04)
48	13.62 (3.23)	1.59 (0.011)	4.702	96.0	1337.33 ± 9.67 (6.95)
49	11.96 (1.67)	1.71 (0.072)	5.046	96.5	1274.95 ± 40.36 (39.83)
50	8.46 (2.54)	1.65 (0.014)	6.884	97.5	1316.36 ± 10.65 (8.32)
51	12.69 (2.10)	1.67 (0.009)	4.663	96.2	1293.23 ± 8.24 (4.96)
52	12.29 (3.80)	1.81 (0.036)	5.202	96.4	1221.03 ± 19.42 (18.36)
53	1.26 (1.05)	1.61 (0.028)	6.582	99.6	1360.47 ± 17.95 (16.61)
54	10.04 (3.20)	1.57 (0.043)	5.527	97.0	1356.57 ± 27.71 (26.87)
55	7.63 (2.23)	1.64 (0.036)	7.594	97.7	1323.08 ± 21.94 (20.90)
56	10.03 (1.31)	1.60 (0.031)	5.692	97.0	1339.35 ± 20.22 (19.07)
57	13.52 (3.17)	1.52 (0.019)	3.994	96.0	1376.81 ± 14.50 (12.78)
58	8.84 (1.34)	1.80 (0.047)	7.194	97.4	1235.67 ± 25.05 (24.22)

Table DR-1
40Ar/39Ar Data for Detrital Muscovites
Burhi Gandaki River - Sample 01WBS3

Analysis Number	$^{36}Ar/^{40}Ar$ $(x10^{-5})^{++}$	$^{39}Ar/^{40}Ar$ $(x10^{-3})^{++}$	$^{39}Ar_K$ $(x10^{-16}$ mol$)^{**}$	$^{40}Ar^*$ $(\%)^{\#}$	Age (Ma)$^{\$}$
1	12.00 (2.74)	2.41 (0.009)	8.837	96.5	972.55 ± 14.29 (2.98)
2	8.46 (1.60)	2.39 (0.039)	12.455	97.5	986.35 ± 18.91 (12.59)
3	11.93 (1.89)	4.74 (0.004)	17.482	96.5	559.30 ± 8.95 (0.46)
4	0.48 (1.34)	2.57 (0.004)	10.811	99.9	950.70 ± 13.77 (1.02)
5	1.11 (1.78)	5.63 (0.014)	18.444	99.7	495.97 ± 8.13 (1.09)
6	14.56 (3.70)	2.36 (0.019)	7.108	95.7	983.03 ± 15.53 (6.54)
7	1.23 (4.82)	2.91 (0.012)	9.652	99.6	860.61 ± 13.04 (2.88)
8	0.16 (1.54)	2.91 (0.006)	8.250	100.0	862.32 ± 12.81 (1.35)
9	0.62 (1.56)	1.86 (0.009)	9.268	99.8	1214.79 ± 16.99 (4.33)
10	2.77 (1.80)	2.61 (0.016)	11.446	99.2	933.51 ± 14.29 (4.55)
11	0.15 (2.95)	1.95 (0.005)	6.411	100.0	1175.46 ± 16.18 (2.05)
12	18.99 (4.32)	1.82 (0.009)	4.808	94.4	1183.62 ± 16.78 (4.64)
13	16.37 (4.10)	2.00 (0.007)	6.092	95.2	1111.07 ± 15.76 (3.27)
14	0.43 (2.45)	1.80 (0.007)	6.984	99.9	1241.60 ± 17.05 (3.51)
15	0.20 (3.81)	2.52 (0.030)	6.915	100.0	967.85 ± 16.48 (8.82)
16	18.68 (2.90)	2.38 (0.013)	6.442	94.5	966.00 ± 14.51 (4.17)
17	12.47 (0.94)	2.59 (0.000)	13.307	96.3	919.99 ± 13.39 (0.15)
18	1.57 (3.35)	1.92 (0.001)	7.791	99.5	1183.86 ± 16.14 (0.35)
19	2.02 (3.33)	2.17 (0.017)	6.989	99.4	1079.51 ± 16.34 (6.24)
20	0.58 (2.97)	3.01 (0.011)	7.660	99.8	839.81 ± 12.71 (2.42)
21	1.91 (0.91)	2.90 (0.000)	14.978	99.4	860.84 ± 12.72 (0.10)
22	0.02 (3.96)	2.11 (0.033)	6.203	100.0	1104.72 ± 20.07 (12.92)
23	3.95 (2.21)	2.10 (0.008)	5.536	98.8	1099.90 ± 15.61 (3.06)
24	11.23 (2.27)	2.24 (0.009)	6.141	96.7	1031.97 ± 14.93 (3.10)
25	2.54 (2.65)	2.05 (0.011)	6.215	99.2	1123.95 ± 16.22 (4.63)
26	2.68 (1.50)	2.37 (0.018)	8.580	99.2	1007.88 ± 15.46 (5.75)
27	12.74 (2.91)	2.66 (0.026)	6.465	96.2	898.28 ± 14.95 (7.12)
28	1.58 (3.62)	2.37 (0.026)	7.503	99.5	1009.85 ± 16.68 (8.46)
29	2.07 (3.39)	2.61 (0.007)	11.246	99.4	935.10 ± 13.70 (1.96)
30	0.92 (2.62)	1.79 (0.018)	8.634	99.7	1246.85 ± 19.07 (9.16)
31	0.08 (1.97)	2.39 (0.017)	7.576	100.0	1008.24 ± 15.33 (5.40)
32	10.91 (2.64)	1.88 (0.021)	6.875	96.8	1178.41 ± 18.86 (9.85)
33	10.02 (2.07)	2.23 (0.008)	8.970	97.0	1037.88 ± 14.95 (2.90)
34	14.82 (3.05)	2.28 (0.014)	6.165	95.6	1007.79 ± 15.21 (5.04)
35	12.32 (2.77)	1.93 (0.014)	6.278	96.4	1148.50 ± 16.95 (6.16)
36	15.55 (4.21)	1.97 (0.008)	5.081	95.4	1124.40 ± 15.98 (3.68)
37	9.38 (1.51)	2.22 (0.014)	9.515	97.2	1044.43 ± 15.58 (5.07)
38	11.96 (3.43)	2.40 (0.009)	8.001	96.5	976.87 ± 14.32 (2.94)
39	13.54 (2.89)	2.07 (0.015)	6.159	96.0	1088.63 ± 16.36 (6.08)
40	12.41 (3.82)	2.05 (0.010)	6.593	96.3	1099.62 ± 15.81 (3.99)
41	0.91 (4.42)	3.10 (0.054)	9.294	99.7	819.46 ± 16.78 (11.47)
42	0.27 (2.24)	2.03 (0.001)	6.556	99.9	1137.79 ± 15.69 (0.44)
43	1.32 (0.64)	2.18 (0.013)	11.432	99.6	1075.62 ± 15.82 (4.85)
44	0.47 (1.48)	2.28 (0.000)	11.743	99.9	1043.50 ± 14.73 (0.10)
45	0.02 (1.13)	3.01 (0.025)	11.516	100.0	841.24 ± 13.72 (5.66)
46	1.93 (2.66)	2.64 (0.024)	10.549	99.4	928.19 ± 15.01 (6.59)
47	1.50 (1.45)	2.77 (0.006)	9.721	99.6	895.05 ± 13.20 (1.52)
48	2.54 (1.12)	2.85 (0.019)	8.948	99.2	873.80 ± 13.66 (4.57)
49	1.41 (1.90)	2.53 (0.015)	12.267	99.6	961.70 ± 14.53 (4.37)
50	2.07 (4.71)	2.35 (0.006)	8.360	99.4	1016.79 ± 14.59 (2.03)

Table DR-1
40Ar/39Ar Data for Detrital Muscovites
Burhi Gandaki River - Sample 01WBS4

Analysis Number	$^{36}Ar/^{40}Ar$ $(x10^{-4})^{++}$	$^{39}Ar/^{40}Ar$ $(x10^{-1})^{++}$	$^{39}Ar_K$ $(x10^{-15}$ mol$)^{**}$	$^{40}Ar^*$ $(\%)^{\#}$	Age (Ma)$^{\$}$
1	2.96 (2.01)	5.31 (0.096)	29.732	91.0	5.53 ± 0.39 (.38)
2	6.31 (1.47)	4.02 (0.081)	45.192	81.2	6.51 ± 0.40 (.38)
3	9.64 (2.48)	3.83 (0.052)	29.038	71.4	6.01 ± 0.63 (.62)
4	10.13 (2.95)	3.88 (0.029)	25.871	69.9	5.81 ± 0.73 (.72)
5	11.73 (2.39)	3.57 (0.024)	21.843	65.2	5.90 ± 0.65 (.64)
6	7.71 (0.75)	3.66 (0.022)	48.025	77.1	6.78 ± 0.24 (.2)
7	11.27 (3.14)	3.65 (0.061)	38.780	66.6	5.88 ± 0.84 (.83)
8	12.60 (1.98)	3.15 (0.059)	37.903	62.7	6.41 ± 0.63 (.62)
9	16.10 (1.41)	2.92 (0.081)	27.779	52.4	5.78 ± 0.54 (.53)
10	6.67 (10.14)	4.61 (0.262)	17.137	80.1	5.60 ± 2.13 (2.12)
11	0.12 (7.17)	3.97 (0.215)	20.022	99.4	8.06 ± 1.77 (1.76)
12	14.77 (9.24)	2.99 (0.118)	13.471	56.3	6.07 ± 2.96 (2.96)
13	3.47 (7.40)	4.61 (0.202)	19.543	89.5	6.27 ± 1.56 (1.55)
14	0.66 (6.22)	3.11 (0.027)	11.322	97.9	10.13 ± 1.90 (1.89)
15	5.81 (4.65)	4.82 (0.223)	46.171	82.6	5.53 ± 0.97 (.96)
16	5.74 (5.34)	3.91 (0.119)	26.461	82.9	6.83 ± 1.32 (1.32)
17	0.56 (13.20)	3.34 (0.128)	7.467	98.2	9.46 ± 3.76 (3.76)
18	8.73 (4.56)	4.01 (0.192)	20.162	74.1	5.95 ± 1.15 (1.14)
19	1.02 (4.71)	4.27 (0.291)	16.692	96.8	7.31 ± 1.17 (1.17)
20	1.80 (1.64)	1.83 (0.010)	19.215	94.6	16.58 ± 0.32 (.09)
21	4.15 (2.02)	1.87 (0.012)	5.741	87.6	15.02 ± 0.30 (.11)
22	1.63 (0.56)	1.94 (0.014)	33.398	95.1	15.76 ± 0.32 (.12)
23	2.90 (0.79)	2.02 (0.015)	15.431	91.3	14.52 ± 0.29 (.12)
24	2.13 (1.54)	1.44 (0.011)	8.030	93.6	20.79 ± 0.42 (.16)
25	5.25 (3.12)	3.27 (0.025)	14.683	84.3	8.31 ± 0.17 (.08)
26	5.47 (2.05)	3.50 (0.010)	13.477	83.7	7.70 ± 0.15 (.03)
27	3.70 (1.09)	3.32 (0.037)	31.760	88.9	8.64 ± 0.19 (.11)
28	1.86 (0.52)	1.95 (0.022)	38.705	94.4	15.59 ± 0.35 (.19)
29	8.96 (1.26)	1.51 (0.014)	9.155	73.5	15.62 ± 0.35 (.2)
30	1.50 (0.67)	2.73 (0.025)	28.225	95.4	11.26 ± 0.24 (.11)
31	2.24 (2.47)	4.52 (0.063)	17.679	93.2	6.64 ± 0.16 (.1)
32	1.48 (0.69)	2.67 (0.017)	23.476	95.5	11.51 ± 0.23 (.07)
33	6.44 (0.65)	3.68 (0.019)	31.024	80.8	7.08 ± 0.14 (.04)
34	0.71 (1.17)	2.63 (0.019)	28.170	97.8	11.97 ± 0.24 (.09)
35	0.73 (1.04)	2.03 (0.016)	21.916	97.7	15.50 ± 0.31 (.12)
36	2.83 (1.95)	4.35 (0.071)	27.250	91.4	6.78 ± 0.17 (.12)
37	5.47 (0.91)	2.39 (0.035)	18.175	83.7	11.27 ± 0.28 (.19)
38	4.07 (2.12)	2.65 (0.019)	11.045	87.9	10.68 ± 0.22 (.09)
39	14.20 (1.58)	3.13 (0.032)	14.838	57.9	5.97 ± 0.15 (.1)
40	6.38 (1.25)	2.57 (0.013)	27.128	81.0	10.15 ± 0.20 (.06)
41	9.26 (1.28)	2.59 (0.016)	18.850	72.5	9.00 ± 0.18 (.08)
42	9.84 (1.40)	3.26 (0.039)	22.324	70.8	6.99 ± 0.18 (.12)
43	11.26 (2.00)	3.37 (0.027)	20.129	66.6	6.37 ± 0.14 (.08)
44	8.80 (0.99)	2.45 (0.028)	18.764	73.9	9.69 ± 0.23 (.15)
45	2.58 (0.35)	0.85 (0.003)	22.221	92.3	34.49 ± 0.65 (.15)
46	0.02 (0.91)	2.55 (0.029)	17.462	99.8	12.59 ± 0.27 (.14)
47	8.47 (1.55)	2.72 (0.011)	21.649	74.9	8.85 ± 0.17 (.05)
48	1.01 (1.56)	2.96 (0.020)	17.634	96.9	10.54 ± 0.21 (.07)
49	6.07 (1.06)	3.58 (0.016)	14.894	81.9	7.00 ± 0.27 (.04)
50	2.42 (0.71)	2.80 (0.017)	25.178	92.7	10.13 ± 0.40 (.07)
51	5.81 (3.65)	2.89 (0.058)	8.046	82.7	8.74 ± 0.40 (.21)
52	2.24 (1.23)	1.80 (0.030)	12.793	93.3	15.79 ± 0.67 (.28)
53	6.24 (1.54)	3.11 (0.038)	7.709	81.4	8.01 ± 0.33 (.12)
54	3.24 (1.27)	3.47 (0.024)	22.295	90.3	7.96 ± 0.31 (.06)
55	7.15 (1.67)	2.43 (0.007)	13.136	78.8	9.93 ± 0.39 (.04)
56	7.34 (1.23)	2.32 (0.046)	6.188	78.2	10.28 ± 0.47 (.26)
57	9.70 (4.65)	4.77 (0.054)	9.399	71.2	4.57 ± 0.19 (.07)
58	2.03 (1.09)	2.99 (0.008)	22.164	93.9	9.60 ± 0.37 (.03)
59	0.66 (0.16)	2.46 (0.026)	42.239	97.9	12.15 ± 0.49 (.13)
60	2.62 (1.00)	2.00 (0.035)	20.739	92.2	14.05 ± 0.60 (.26)
61	5.20 (1.43)	2.35 (0.055)	15.079	84.5	10.98 ± 0.52 (.3)
62	0.52 (2.51)	3.88 (0.055)	17.647	98.3	7.76 ± 0.32 (.11)
63	6.94 (2.06)	3.66 (0.051)	17.594	79.4	6.63 ± 0.28 (.12)
64	0.51 (0.37)	1.83 (0.026)	29.693	98.4	16.41 ± 0.68 (.23)
65	0.37 (1.86)	4.76 (0.084)	20.042	98.7	6.35 ± 0.27 (.11)
66	0.36 (0.09)	0.98 (0.006)	17.261	98.9	30.72 ± 1.20 (.19)
67	2.20 (0.90)	2.06 (0.035)	6.641	93.4	13.82 ± 0.59 (.25)
68	0.50 (0.54)	1.38 (0.014)	26.406	98.5	21.66 ± 0.87 (.23)

Table DR-1
40Ar/39Ar Data for Detrital Muscovites
Burhi Gandaki River - Sample 01WBS5

Analysis Number	$^{36}Ar/^{40}Ar$ $(x10^{-4})^{++}$	$^{39}Ar/^{40}Ar$ $(x10^{-1})^{++}$	$^{39}Ar_K$ $(x10^{-15}$ mol$)^{**}$	$^{40}Ar^*$ $(\%)^{\#}$	Age $(Ma)^{\$}$
1	10.28 (5.62)	5.04 (0.037)	4.808	69.5	4.23 ± 0.17 (.05)
2	12.28 (8.06)	4.92 (0.011)	6.304	63.6	3.96 ± 0.15 (.01)
3	13.43 (7.74)	6.20 (0.039)	5.558	60.1	2.98 ± 0.12 (.03)
4	10.76 (18.36)	4.80 (0.051)	1.924	68.0	4.34 ± 0.18 (.07)
5	10.34 (8.25)	5.34 (0.019)	4.788	69.3	3.98 ± 0.16 (.02)
6	9.04 (2.54)	4.06 (0.020)	6.217	73.1	5.52 ± 0.22 (.04)
7	3.12 (3.49)	3.41 (0.021)	4.943	90.6	8.12 ± 0.32 (.05)
8	3.47 (3.31)	3.19 (0.048)	6.386	89.6	8.58 ± 0.36 (.14)
9	3.44 (4.10)	1.89 (0.013)	4.291	89.7	14.46 ± 0.57 (.11)
10	9.53 (9.08)	5.20 (0.043)	3.909	71.7	4.22 ± 0.17 (.05)
11	14.93 (8.70)	4.48 (0.030)	4.939	55.8	3.82 ± 0.15 (.05)
12	14.52 (18.43)	5.45 (0.040)	3.878	56.9	3.20 ± 0.13 (.04)
13	16.53 (15.12)	3.34 (0.085)	6.463	51.1	4.69 ± 4.10 (4.09)
14	14.89 (4.15)	3.83 (0.035)	17.047	55.9	4.47 ± 1.00 (.98)
15	14.96 (4.80)	2.63 (0.013)	13.808	55.7	6.49 ± 1.67 (1.65)
16	10.29 (8.87)	3.39 (0.055)	11.250	69.5	6.27 ± 2.38 (2.36)
17	8.85 (9.02)	2.68 (0.029)	4.077	73.7	8.42 ± 3.05 (3.03)
18	15.29 (7.52)	2.44 (0.049)	5.925	54.8	6.85 ± 2.79 (2.78)
19	3.14 (2.46)	3.96 (0.032)	21.858	90.5	7.00 ± 0.62 (.56)
20	9.74 (4.59)	2.75 (0.034)	9.768	71.1	7.92 ± 1.54 (1.51)
21	11.17 (3.65)	2.47 (0.035)	8.886	66.9	8.28 ± 1.38 (1.34)
22	8.74 (2.61)	3.79 (0.024)	18.049	74.0	5.98 ± 0.66 (.62)
23	9.36 (3.82)	2.42 (0.018)	13.438	72.3	9.12 ± 1.47 (1.42)
24	11.38 (4.98)	1.63 (0.052)	7.093	66.3	12.40 ± 2.84 (2.8)
25	0.09 (6.86)	3.84 (0.050)	12.290	99.5	7.94 ± 1.64 (1.61)
26	5.14 (11.56)	3.50 (0.113)	7.248	84.7	7.39 ± 3.00 (2.98)
27	6.64 (4.43)	3.87 (0.033)	25.047	80.2	6.34 ± 1.06 (1.03)
28	7.88 (5.08)	3.05 (0.033)	13.747	76.6	7.68 ± 1.53 (1.5)
29	7.45 (2.85)	2.85 (0.017)	29.345	77.9	8.35 ± 0.96 (.9)
30	14.42 (3.73)	1.88 (0.005)	9.891	57.3	9.30 ± 1.82 (1.78)
31	9.74 (2.15)	2.53 (0.045)	20.600	71.1	8.59 ± 0.86 (.79)
32	13.60 (5.07)	1.41 (0.035)	6.611	59.8	12.94 ± 3.30 (3.26)
33	13.88 (8.41)	2.56 (0.072)	10.283	58.9	7.04 ± 2.99 (2.98)
34	13.33 (4.93)	2.53 (0.032)	11.773	60.5	7.32 ± 1.78 (1.76)
35	2.29 (17.79)	2.86 (0.074)	3.923	93.1	9.97 ± 5.62 (5.61)

Table DR-1
40Ar/39Ar Data for Detrital Muscovites
Burhi Gandaki River - Sample 01WBS6

Analysis Number	$^{36}Ar/^{40}Ar$ $(x10^{-4})^{++}$	$^{39}Ar/^{40}Ar$ $(x10^{-1})^{++}$	$^{39}Ar_K$ $(x10^{-15}$ mol$)^{**}$	$^{40}Ar^*$ $(\%)^{\#}$	Age $(Ma)^{\$}$
1	0.61 (3.18)	1.51 (0.040)	13.310	98.1	19.78 ± 2.10 (1.96)
2	1.30 (3.03)	1.56 (0.014)	9.740	96.1	18.76 ± 1.89 (1.75)
3	2.14 (4.02)	2.09 (0.023)	12.217	93.6	13.66 ± 1.81 (1.73)
4	9.52 (5.33)	2.64 (0.046)	13.525	71.8	8.30 ± 1.85 (1.83)
5	9.48 (4.36)	1.95 (0.022)	9.454	71.9	11.23 ± 2.06 (2.01)
6	5.61 (4.34)	1.95 (0.019)	8.198	83.3	13.03 ± 2.06 (2.)
7	10.81 (3.42)	2.59 (0.074)	12.280	68.0	8.04 ± 1.27 (1.23)
8	7.09 (1.45)	1.83 (0.017)	12.336	79.0	13.18 ± 0.89 (.72)
9	12.37 (2.86)	1.42 (0.007)	5.996	63.4	13.58 ± 1.88 (1.8)
10	2.31 (8.09)	3.65 (0.112)	8.054	93.0	7.79 ± 2.03 (2.01)
11	5.64 (4.16)	2.74 (0.107)	14.708	83.2	9.27 ± 1.47 (1.43)
12	15.15 (2.81)	1.99 (0.053)	15.856	55.2	8.46 ± 1.36 (1.32)
13	5.47 (1.76)	2.35 (0.022)	44.003	83.7	10.88 ± 0.80 (.68)
14	6.88 (1.99)	1.56 (0.053)	22.813	79.6	15.53 ± 1.44 (1.31)
15	5.64 (1.83)	1.85 (0.030)	42.324	83.2	13.74 ± 1.07 (.93)
16	8.38 (1.23)	1.54 (0.031)	29.191	75.2	14.85 ± 0.99 (.81)
17	10.56 (2.60)	1.33 (0.014)	23.203	68.7	15.73 ± 1.87 (1.77)
18	14.69 (3.33)	2.72 (0.037)	30.904	56.5	6.37 ± 1.14 (1.11)

Table DR-1
40Ar/39Ar Data for Detrital Muscovites
Burhi Gandaki River - Sample 01WBS7

Analysis Number	$^{36}Ar/^{40}Ar$ $(x10^{-4})^{++}$	$^{39}Ar/^{40}Ar$ $(x10^{-1})^{++}$	$^{39}Ar_K$ $(x10^{-15}$ mol$)^{**}$	$^{40}Ar^*$ $(\%)^{\#}$	Age $(Ma)^{\$}$
1	7.32 (1.76)	0.91 (0.009)	7.737	78.3	26.09 ± 1.06 (.34)
2	1.63 (7.17)	2.13 (0.035)	3.863	95.1	13.62 ± 0.58 (.23)
3	0.40 (2.91)	1.06 (0.010)	4.182	98.8	28.39 ± 1.12 (.26)
4	4.82 (2.77)	1.20 (0.006)	2.609	85.7	21.81 ± 0.85 (.13)
5	1.08 (3.14)	2.12 (0.030)	3.135	96.7	13.95 ± 0.58 (.21)
6	0.12 (0.38)	0.26 (0.002)	7.141	99.6	113.81 ± 4.34 (.74)
7	16.73 (3.45)	2.08 (0.030)	8.015	50.5	7.42 ± 0.35 (.21)
8	0.25 (1.31)	0.94 (0.008)	9.296	99.2	31.95 ± 1.26 (.27)
9	6.68 (11.74)	3.32 (0.069)	2.700	80.1	7.39 ± 0.34 (.19)
10	0.54 (8.03)	1.69 (0.025)	3.128	98.3	17.74 ± 0.73 (.26)
11	0.77 (4.43)	4.31 (0.049)	16.586	97.5	6.93 ± 0.28 (.08)
12	3.03 (4.15)	5.09 (0.101)	15.111	90.8	5.47 ± 0.24 (.12)
13	9.52 (7.11)	4.84 (0.092)	9.407	71.7	4.53 ± 0.21 (.12)
14	10.14 (3.52)	5.03 (0.129)	10.324	69.9	4.26 ± 0.23 (.16)
15	0.88 (10.31)	5.22 (0.025)	7.119	97.1	5.70 ± 0.22 (.03)
16	1.65 (2.00)	2.03 (0.007)	9.153	95.0	14.31 ± 0.56 (.05)
17	3.12 (3.49)	3.24 (0.018)	6.880	90.6	8.56 ± 0.34 (.05)
18	0.45 (4.31)	3.06 (0.008)	8.722	98.5	9.84 ± 0.38 (.03)
19	2.17 (3.54)	3.59 (0.042)	8.803	93.4	7.96 ± 0.32 (.1)
20	5.44 (5.27)	4.45 (0.047)	6.900	83.8	5.77 ± 0.23 (.07)
21	0.85 (6.32)	4.90 (0.023)	6.547	97.2	6.08 ± 0.24 (.03)
22	2.91 (9.03)	4.50 (0.051)	8.013	91.2	6.20 ± 0.25 (.08)
23	1.82 (2.51)	3.93 (0.066)	9.093	94.4	7.35 ± 0.31 (.13)
24	3.53 (9.19)	4.63 (0.028)	4.426	89.3	5.91 ± 0.23 (.04)
25	0.28 (0.60)	0.45 (0.005)	6.238	99.1	66.91 ± 2.65 (.73)
26	0.34 (0.93)	0.89 (0.011)	7.176	99.0	33.80 ± 1.37 (.43)
27	4.67 (4.28)	4.43 (0.012)	7.914	86.0	5.95 ± 0.23 (.02)
28	0.17 (12.96)	4.96 (0.025)	7.190	99.3	6.13 ± 0.24 (.03)
29	3.84 (5.73)	5.35 (0.061)	7.799	88.4	5.06 ± 0.21 (.07)
30	2.13 (9.61)	3.24 (0.012)	4.355	93.6	8.84 ± 0.34 (.03)
31	0.70 (4.39)	4.80 (0.089)	11.820	97.7	6.24 ± 0.27 (.12)
32	5.26 (25.13)	5.48 (0.117)	1.915	84.2	4.71 ± 0.22 (.12)

Table DR-1
40Ar/39Ar Data for Detrital Muscovites
Burhi Gandaki River - Sample 01WBS8

Analysis Number	$^{36}Ar/^{40}Ar$ $(x10^{-5})^{++}$	$^{39}Ar/^{40}Ar$ $(x10^{-3})^{++}$	$^{39}Ar_K$ $(x10^{-16}$ mol$)^{**}$	$^{40}Ar^*$ $(\%)^{\#}$	Age $(Ma)^{\$}$
1	34.49 (3.17)	8.48 (0.115)	21.282	89.8	317.45 ± 4.85 (4.39)
2	33.19 (5.12)	6.23 (0.053)	16.234	90.2	421.09 ± 4.45 (3.55)
3	32.71 (4.42)	2.93 (0.046)	7.754	90.3	801.83 ± 12.12 (11.21)
4	26.38 (2.23)	5.85 (0.060)	19.216	92.2	454.03 ± 5.27 (4.43)
5	38.95 (5.08)	4.52 (0.073)	10.044	88.5	548.65 ± 9.28 (8.65)
6	34.07 (6.37)	7.61 (0.017)	19.354	89.9	350.67 ± 2.40 (0.79)
7	27.27 (2.84)	7.03 (0.084)	22.328	91.9	384.41 ± 5.15 (4.52)
8	26.91 (1.14)	4.33 (0.081)	13.929	92.0	589.25 ± 10.81 (10.20)
9	27.42 (1.99)	9.51 (0.062)	30.019	91.9	291.88 ± 2.70 (1.90)
10	30.43 (5.68)	12.49 (0.230)	35.529	91.0	224.33 ± 4.52 (4.26)
11	26.11 (1.43)	10.31 (0.094)	28.873	92.3	271.75 ± 3.07 (2.48)
12	31.01 (7.04)	6.41 (0.220)	15.113	90.8	412.99 ± 14.20 (13.96)
13	21.30 (4.87)	3.06 (0.009)	10.453	93.7	797.02 ± 5.03 (2.07)
14	18.40 (2.53)	3.65 (0.050)	14.456	94.6	696.50 ± 9.35 (8.40)
15	25.47 (5.12)	5.88 (0.016)	16.834	92.5	453.22 ± 3.08 (1.15)
16	22.07 (1.32)	7.67 (0.100)	25.382	93.5	360.87 ± 5.12 (4.56)
17	31.37 (3.88)	6.66 (0.084)	15.515	90.7	398.88 ± 5.58 (4.96)
18	22.97 (1.08)	5.59 (0.060)	17.764	93.2	477.19 ± 5.65 (4.80)
19	30.16 (3.48)	3.53 (0.038)	8.510	91.1	693.35 ± 7.91 (6.77)
20	23.84 (3.48)	12.75 (0.047)	39.069	93.0	224.41 ± 1.72 (0.84)
21	0.47 (1.77)	6.12 (0.015)	21.644	99.9	468.02 ± 3.10 (1.00)
22	0.89 (0.75)	6.60 (0.044)	21.789	99.7	437.48 ± 3.79 (2.60)
23	1.06 (3.77)	11.70 (0.082)	28.267	99.7	259.62 ± 2.42 (1.70)
24	0.74 (2.88)	6.70 (0.067)	20.039	99.8	432.05 ± 4.73 (3.85)
25	1.26 (1.62)	7.07 (0.047)	21.905	99.6	410.97 ± 3.60 (2.47)
26	1.86 (2.38)	5.95 (0.042)	18.012	99.4	478.46 ± 4.21 (2.96)
27	1.21 (1.91)	6.09 (0.030)	18.363	99.6	469.64 ± 3.60 (2.07)
28	1.26 (1.17)	7.17 (0.077)	34.598	99.6	406.08 ± 4.69 (3.91)
29	1.66 (2.19)	6.86 (0.113)	24.879	99.5	421.93 ± 6.78 (6.23)
30	1.61 (2.00)	7.69 (0.076)	27.277	99.5	380.92 ± 4.21 (3.42)
31	9.81 (3.72)	6.63 (0.036)	20.303	97.1	425.58 ± 3.43 (2.11)
32	7.17 (1.70)	5.39 (0.051)	22.584	97.9	514.27 ± 5.37 (4.32)
33	9.62 (3.94)	6.68 (0.065)	20.877	97.2	422.65 ± 4.65 (3.79)
34	9.26 (2.35)	8.17 (0.107)	26.490	97.3	353.01 ± 4.89 (4.32)
35	7.12 (1.04)	7.33 (0.003)	30.887	97.9	391.82 ± 2.51 (0.17)
36	13.42 (3.74)	8.99 (0.007)	20.169	96.0	320.03 ± 2.10 (0.25)
37	10.26 (4.02)	6.16 (0.060)	17.934	97.0	453.54 ± 4.93 (4.02)
38	3.25 (0.48)	8.56 (0.020)	28.201	99.0	344.21 ± 2.36 (0.75)
39	0.15 (3.50)	7.33 (0.062)	18.656	100.0	399.40 ± 3.96 (3.03)
40	0.50 (2.21)	6.90 (0.059)	31.323	99.8	421.04 ± 4.18 (3.21)
41	10.81 (2.53)	9.65 (0.078)	26.532	96.8	302.02 ± 3.06 (2.34)
42	0.26 (2.60)	5.79 (0.036)	19.472	99.9	491.58 ± 4.05 (2.64)
43	2.96 (1.71)	8.85 (0.104)	27.792	99.1	334.04 ± 4.21 (3.60)
44	0.82 (2.73)	7.64 (0.089)	24.452	99.8	384.04 ± 4.73 (4.04)
45	0.14 (1.74)	6.62 (0.050)	16.696	100.0	437.14 ± 4.04 (2.94)
46	0.40 (0.96)	5.16 (0.037)	22.302	99.9	543.37 ± 4.74 (3.36)
47	0.85 (3.50)	7.07 (0.047)	16.891	99.7	411.76 ± 3.60 (2.46)
48	1.61 (2.16)	10.53 (0.021)	34.564	99.5	285.75 ± 1.95 (0.52)
49	0.58 (2.30)	7.69 (0.033)	28.240	99.8	382.13 ± 2.86 (1.47)
50	1.27 (3.48)	6.88 (0.030)	20.673	99.6	421.13 ± 3.15 (1.66)
51	6.43 (0.65)	6.48 (0.001)	33.422	98.1	438.08 ± 2.77 (0.05)
52	0.18 (0.53)	6.64 (0.002)	24.177	99.9	436.14 ± 2.76 (0.13)
53	7.73 (1.26)	6.70 (0.047)	28.723	97.7	423.97 ± 3.83 (2.73)
54	0.12 (2.09)	7.98 (0.033)	30.138	100.0	369.75 ± 2.76 (1.40)
55	9.42 (1.71)	7.20 (0.059)	25.345	97.2	395.81 ± 3.93 (3.00)
56	10.07 (1.80)	6.72 (0.046)	22.183	97.0	420.23 ± 3.78 (2.67)
57	0.92 (1.66)	7.08 (0.032)	31.305	99.7	411.09 ± 3.10 (1.65)
58	2.55 (1.01)	15.05 (0.177)	39.463	99.2	204.15 ± 2.67 (2.29)
59	0.28 (3.87)	8.71 (0.059)	28.545	99.9	341.47 ± 3.06 (2.12)

Notes:

$^{++}$: Numbers in parenthesis indicate 2 σ error on individual measurements.

**: Number of moles of K-derived ^{39}Ar ($^{39}Ar_K$)released for each analysis

$^{\#}$: Percentage of radiogenic ^{40}Ar ($^{40}Ar^*$) in the total ^{40}Ar for each analysis

$^{\$}$: Uncertainties include propagated error in the irradiation parameter, J. Uncertainties in parenthesis represent the contribution of analytical error to the total uncertainty.

Taylor creek sanidine (28.34 $\pm$ 0.16 Ma) was used as a neutron flux monitor for all analyses (see Renne et al., 1998; *Chemical Geology* v. 145, p. 117-152)

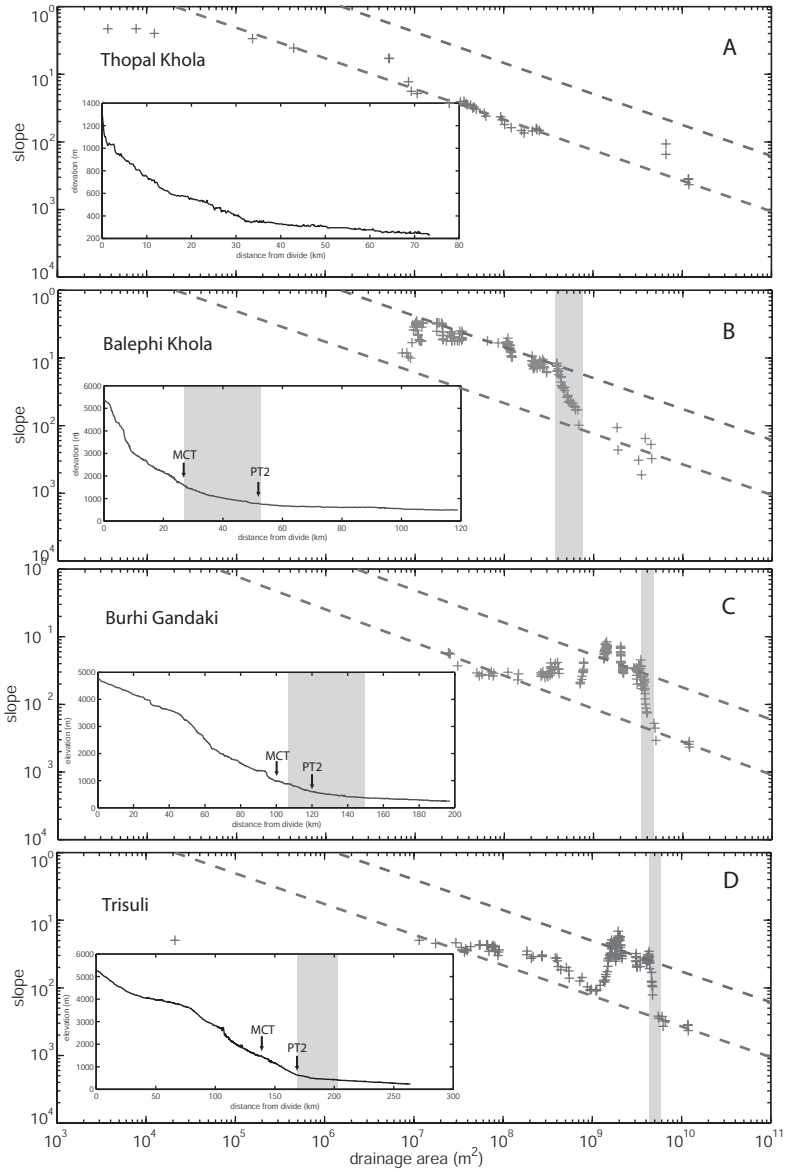

Figure DR-1: Stream profiles from four representative tributaries in central Nepal. A: Thopal Khola, sourced below PT2; B: Balephi Khola, sourced above PT2; C: Burhi Gandaki trunk stream, sourced above STF. D: Trisuli trunk stream, sourced above STF Dashed lines show upper and lower bounds of steepness values for a reference concavity of 0.45, determined from superposition of all data from the 56 tributaries analyzed (see text). Grey bands in Balephi, Burhi Gandaki and Trisuli rivers show zones of locally high concavity, interpreted as the distance over which rock uplift rates are increasing across PT2. Location of channel heads for stream profiles are shown in Figure 3.

Wobus et al., Figure DR-1